Wall Pressure Fluctuations in a Three-Dimensional Shock-Wave/Turbulent Boundary Interaction

D. K. M. Tan,* T. T. Tran,† and S. M. Bogdonoff‡
Princeton University, Princeton, New Jersey

Surface pressure fluctuations have been measured in a three-dimensional shock-wave/turbulent boundary-layer interaction. The shock wave was generated by a sharp-edged fin set perpendicular to the boundary layer at 10 deg to the flow direction. Tests were conducted at a nominal freestream Mach number of 3. The pressure fluctuations were found to be small through the interaction, with only a twofold increase from upstream values. This, however, does not suggest that the flow is steady. Cross-correlation analysis suggests some degree of unsteadiness in the shock structure. Contour plots of the space correlations and maxima in cross correlations were also deduced. The contours showed the development of the spatial scales and decay rates of the pressure producing structures through the interaction.

Nomenclature

C_f = skin-friction coefficient
f = frequency, Hz
N = number of records, each containing 256 data points
$\overline{P}_w$ = mean static pressure, $= (1/n)\sum_{i=1}^{n} P_{wi}$, where n is the number of data points averaged
P_0 = stagnation pressure
q = dynamic pressure
r = active radius of transducer
$R(\xi_1, \xi_2, \tau)$ = space-time correlation, $= [(1/n)\sum_{i=1}^{n} P'_{wi}(x, y, t_i) P'_{w2}(x+\xi_1, y+\xi_2, t_i+\tau)]/(\sigma_{pw1}\sigma_{pw2})$ where $P'_w = P_w - \overline{P}_w$ and $\sigma_{pw} = [(1/n)\sum_{i=1}^{n}(P'_{wi})^2]^{\frac{1}{2}}$
U_c = convection velocity in the flow direction, m/s
U_m = measured convection velocity, m/s
U_τ = shear velocity
X = longitudinal distance
Y = transverse distance
β = $\tan^{-1}\xi_2/\xi_1$
δ_0 = incoming boundary-layer thickness, m
δ_r^* = incoming boundary-layer displacement thickness, m
ν = kinematic viscosity
σ_p = rms of fluctuating pressure signal
θ = momentum thickness, m
τ = time delay
τ_w = wall shear stress
ω = frequency, rad/s
ξ = separation distance between transducers

Subscripts

1 = component in X direction
2 = component in Y direction
e = freestream edge conditions
s = referenced to calculated inviscid shock position
w = values at wall based on incoming freestream conditions

Introduction

THE interaction of a shock wave with a turbulent boundary layer has been the subject of extensive research due to its practical importance as well as intrinsic interest in the problem as a physical phenomenon. However, our knowledge of three-dimensional interactions lags behind our knowledge of the two-dimensional cases, where numerous mean flow and turbulence measurements have been made. This lack of understanding stems from the general complexity of the flows and from the difficulty of performing experimental measurements in such flows. Problems are often encountered when applying familiar experimental techniques used in two-dimensional flows to three-dimensional cases and in interpreting any results obtained unambiguously.

To date, experiments in three-dimensional interactions have been confined mainly to surface flow visualization, surface static pressure, and heat-transfer measurements and, in a few instances, to mean flowfield surveys. There is a lack of data on turbulent quantities, which are necessary since mean flow quantities by themselves do not usually give an adequate understanding of the flowfield physics.

This paper presents measurements of the wall pressure fluctuations generated by an oblique shock-wave/boundary-layer interaction. The pressure fluctuations are, in part, the "footprints" of the turbulence structures in the boundary layer and may therefore not only give information on the shock/boundary-layer interaction, but may also provide an insight into the turbulence behavior in a three-dimensional flow. The configuration is also one of the simplest three-dimensional interactions and has been the subject of many experimental (e.g., McCabe,[1] Stanbrook,[2] Kubota and Stollery,[3] Peake,[4] and Oskam et al.[5]) and analytical and computational studies (e.g., Korkegi,[6] Horstman,[7] Knight,[8] and Stalker[9]).

The shock was generated by a sharp-edged fin set perpendicular to the boundary layer at 10 deg to the flow direction. The boundary layer experienced effects due to the shock wave, pressure gradient, and transverse shear. A 10 deg angle was selected since it produced a relatively weak interaction and since other experimental data already existed for this angle, in particular the mean flowfield data of Oskam et al.[5]

Presented as Paper 85-0125 at the AIAA 23rd Aerospace Sciences Meeting, Reno, NV, Jan. 14-17, 1985; received March 15, 1985; revision received March 6, 1986. Copyright © American Institute of Aeronautics and Astronautics, Inc., 1985. All rights reserved.

*Research Associate, Gas Dynamics Laboratory, Mechanical and Aerospace Engineering Department; presently with Flow Industries, Inc., Kent, WA. Member AIAA.

†Graduate Student, Gas Dynamics Laboratory, Mechanical and Aerospace Engineering Department.

‡Professor, Gas Dynamics Laboratory, Mechanical and Aerospace Engineering Department. Fellow AIAA.

Experimental Method and Conditions

All tests were conducted in the Princeton University 203 $\times$ 203 mm high Reynolds number supersonic blowdown wind tunnel. The 292 mm long, 140 mm high sharp-edged fin was sting-mounted onto the tunnel floor at an angle of 10 ± 0.5 deg to the freestream direction. The fin was braced vertically and horizontally to prevent flutter. The leading edge of the fin was 216 mm downstream of the nozzle exit plane. Figure 1 shows the experimental configuration.

All tests were conducted at a stagnation pressure of 6.9×10^5 N $\cdot$ m^{-2} $\pm$ 1% and a stagnation temperature of 252 K $\pm$ 2%. The Mach number at the test station was 2.95 $\pm$ 1.5% and was uniform across the test section. The freestream unit Reynolds number based on these conditions was 7.2×10^7/m and the wall condition was approximately adiabatic. The incoming boundary layer was a fully turbulent, two-dimensional equilibrium one with transition occurring naturally upstream of the sonic throat. δ_0, δ_r^*, and θ were 0.0153, 0.004, and 0.000753 m, respectively (at $X_s = -117$ mm).

Figure 2 shows the mean surface flow pattern obtained with the kerosene/lampblack technique; this is described in detail by Settles and Teng.[10] It is identical to that obtained by Oskam et al.[5] and was used to aid in the selection of appropriate locations for the pressure measurements. Mean surface static pressures were measured by four streamwise rows of taps. This served as a comparison with the results of Oskam et al.[5] and also as a check against the mean pressures given by the fluctuating pressure transducers.

Measurement of wall pressure fluctuations were made with four miniature differential pressure transducers manufactured by Kulite Semiconductor Products, model XCQ-062-25-D. Each transducer has a 0.71 mm diameter silicon sensing diaphragm on which a fully active Wheatstone bridge is bonded atomically. The natural frequency quoted by the manufacturer is approximately 500 kHz. The transducers were calibrated statically at the operating temperature, i.e., the tunnel was run to cool it before calibration. Shock tube tests by Raman[11] have shown that transducers of this type have dynamic calibrations only a few percent lower than those obtained statically. Calibrations were performed after every six runs, of approximately 30 s duration each. The calibrations were found to differ by only 4% throughout the day.

The four transducers were mounted in-line, 0.2 in. apart, in a cylindrical plug that was fitted into a rotatable eccentric window mounted flush with the tunnel floor. This allowed easy positioning of the plug and also allowed the transducers to be yawed relative to the flow. The transducers were adjusted under a microscope to be flush to less then $0.002\delta_0$ under the plug surface, which minimizes any interference effects on the flow; see Hanly[12] for details.

The signals from each transducer were amplified by a two-stage amplifier circuit (-3 dB points of 120 kHz) at gains of 2000 or 4000. The signals were then low-pass filtered at half the sampling rate by Ithaco 4213 electronic filters. For all fluctuating measurements, the signals were also high-pass filtered at 250 Hz to reduce electronic noise and low-frequency tunnel vibrations. The rms noise in the system without the tunnel running was found to be 13 N $\cdot$ m^{-2}, equivalent to approximately 5% of the upstream rms pressure fluctuation level.

The signals were digitized at a rate of 200 kHz by a Preston GMAD-1 A/D converter, which had a resolution of 8192 counts between -10 and $+10$ V. With a typical transducer sensitivity of 2.5 mV/psi, this gave a resolution of 3.37 and 1.68 N $\cdot$ m^{-2} for gain settings of 2000 and 4000, respectively. Data were obtained in files of N records with 256 sample points per channel per record. Convergence of mean pressure $\bar{P}_w$, rms pressure σ_{pw}, probability density distribution, and power spectra were achieved when $N \geq 100$. In all cases, averages of 200 records were taken.

Phase shifts between the channels were determined by bench testing the circuits and by rotating the plug by 180 deg at the same position in the flow and comparing the cross correlations. A maximum shift of 2 μs was observed between channels, i.e., the location of the maxima in cross correlation differed by a maximum of 2 μs when the plug was rotated.

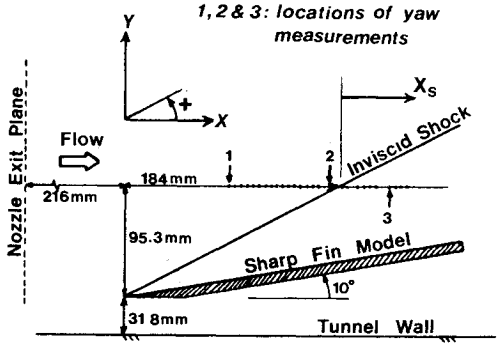

Fig. 1 Diagram indicating survey locations and coordinate system used.

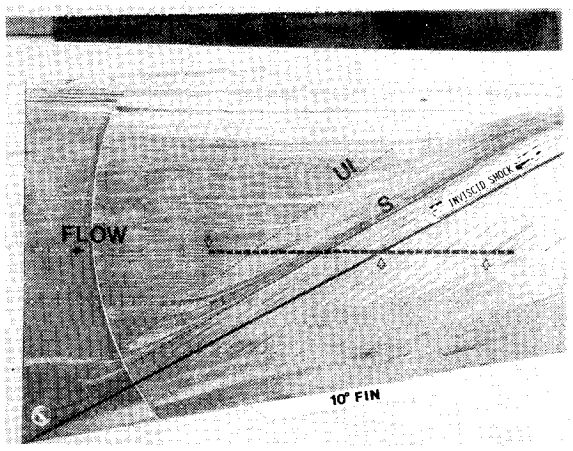

Fig. 2 Surface flow pattern.

It should be noted that the transducers were not referenced to vacuum but to an average of the local mean pressures at each plug position. This allowed high amplifier gains to be used without ac coupling of the signals.

Narrow band analyses of the signals were also conducted by filtering the pressure signals into one-third octave frequency bands. The filtering was performed digitally with a finite-impulse response filter.[13] This class of filter has a linear phase response that ensures no phase shift between the frequencies in the pass band. Unfortunately, there was insufficient resolution in the data to obtain results in frequency bands above 36 kHz.

Fluctuating pressures were measured along a longitudinal line at $Y = 95.3$ mm from the leading edge of the fin; the survey positions and the coordinate system used are shown in Fig. 1. At this Y position, the calculated inviscid shock is located 184 mm from the fin leading edge. All longitudinal dimensions will be referenced to the calculated shock position.

Measurements were also taken with the Kulite plug yawed at various angles to the flow. Three locations were selected for these "yaw" measurements: in the undisturbed upstream position, in the interaction region, and downstream of the interaction region. These positions are also indicated in Fig. 1. Note that the rotations were centered at the first transducer and that the displacements quoted for the cross-correlation results are those of the upstream transducer.

Results and Discussion

Incoming Boundary Layer

The mean wall pressure $\bar{P}_{w\infty}$ for the incoming boundary layer (at $X_s = -117$ mm) was 2.98 $\pm$ 0.05 psi and the normal-

ized rms wall pressure fluctuation $\sigma_{pw}/\bar{P}_{w\infty}$ was 0.013 $\pm$0.0005. The rms value is normally nondimensionalized by the dynamic pressure q_e or the wall shear stress τ_w. The present results gave $\sigma_{pw}/q_e = 0.0021$ and $\sigma_{pw}/\tau_w = 1.85$. These values are about half of those of Kistler and Chen,[14] but are in good agreement with those of Speaker and Ailman,[15] Chu and Hanly,[16] and Coe[17] (see the last two references and Laganelli et al.[18] for comparisons of the fluctuating pressure levels from various authors). Note that measurements were also taken without high-pass filtering of the signals. It was found that the unfiltered rms pressure levels differed by up to 9% from the high-pass filtered levels (a significant portion of this would be due to noise). The values presented here are those that have been high-pass filtered.

The values are probably still too low, however, due to the lack of resolution of the higher frequencies. According to Schewe,[19] the present transducers would give an rms pressure about 60% of that given by an "ideal" transducer. The ideal transducer would have a nondimensional diameter $2rU_c/\nu_w$ of 20, where r is the radius of the transducer. The present transducers have a nondimensional diameter of approximately 200. However, they do capture a significant portion of the spectrum. From Corcos,[20] the maximum measurable frequency by a transducer is given by $2\pi fr/U_c = 1$, where f is the frequency and U_c the convection velocity. For the present transducers, this gives a value of 150 kHz for a U_c of 0.6 U_∞. A typical frequency of the large eddies in this experiment is 37 kHz (U_∞/δ_0).

Space-time correlations $R(\xi_1, \xi_2, \tau)$ were also obtained according to the definition given in the nomenclature; ξ_1 and ξ_2 are the x and y components, respectively, of the distance between the transducers. As observed by other researchers, the maxima of the space-time correlations decrease with increasing separation. Broadband convection velocities U_c were also deduced from the maxima of the space-time correlations. The peaks of the space-time correlations, broadband convection velocities, and longitudinal and transverse space correlations [i.e., $R(\xi_1, 0, 0)$ and $R(0, \xi_2, 0)$, respectively] are shown in Figs. 3-5, together with the results obtained by other researchers.

The maxima of the space-time correlations and convection velocities agree well with values obtained by other workers, but the space correlations are appreciably larger. The larger values of space correlations are probably caused by the lack of resolution of the finer scales, i.e., higher-frequency motions. Therefore, the data would be biased toward the larger structures having higher convection velocities. Note, however, that the results have been made dimensionless by δ_r^*; thus, it is questionable where δ_r^* is an appropriate length scale in both subsonic and supersonic flows, since there is no evidence that it is related to the large-eddy lifetime.

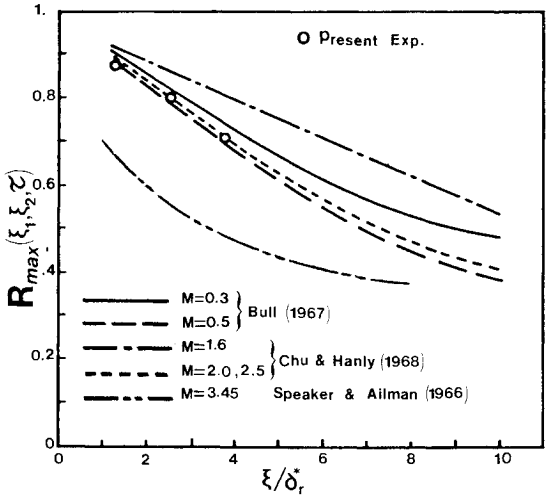

Fig. 3 Maxima of space-time correlation of incoming boundary layer (lines of best fit drawn to data of previous workers).

Mean and Rms Pressure Distributions

The mean static pressure distribution along the survey line ($Y = 95.3$ mm) is shown in Fig. 6. It agrees well with the previous measurements of Oskam et al.[5] The pressure begins to increase at a distance of $18\delta_r^*$ ahead of the calculated shock position, continues to increase over a distance of about $11\delta_r^*$, and levels off to a plateau for about $11\delta_r^*$ before increasing again. This relatively gradual rise in pressure occurs because the shock bifurcates at about a distance of $2.5\delta_0$ above the tunnel floor (see Oskam et al.[5]).

The rms pressure fluctuations along this streamwise line is shown in Fig. 7. We observe an increase from the normalized upstream value of about 0.013 to a value of 0.024 near the point of inflection of the mean static pressure. Note that, in two-dimensional compression corner interactions, a peak in the rms pressure distribution is often observed at the point of inflection of the mean pressure rise; for example, Fig. 8 shows the results of Dolling and Or[21] for a 12 deg corner. This

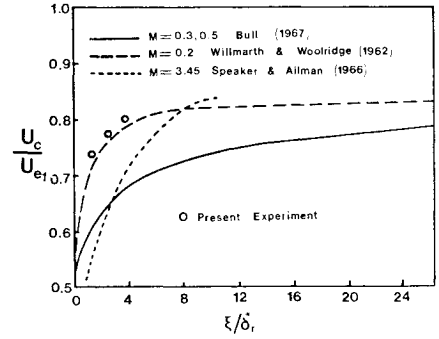

Fig. 4 Broadband convection velocities of the incoming boundary layer.

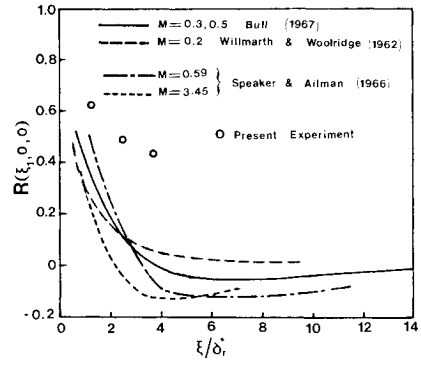

Fig. 5a Longitudinal space correlation ($\tau = 0$) of incoming boundary layer.

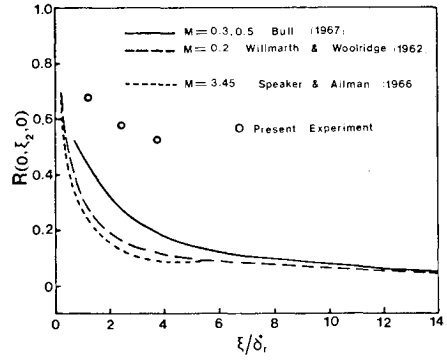

Fig. 5b Transverse space correlation of incoming boundary layer.

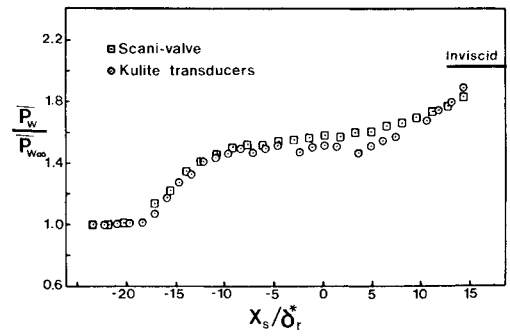

Fig. 6 Mean wall pressure distribution along $Y = 95.3$ mm.

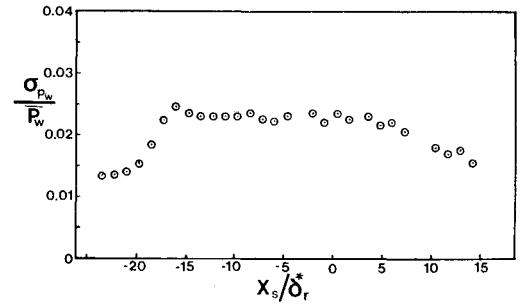

Fig. 7 Rms pressure fluctuations along $Y = 95.3$ mm.

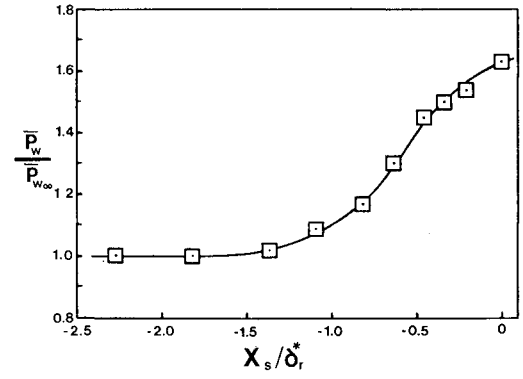

Fig. 8a Mean wall pressure distribution for a 12 deg compression corner (from Ref. 21).

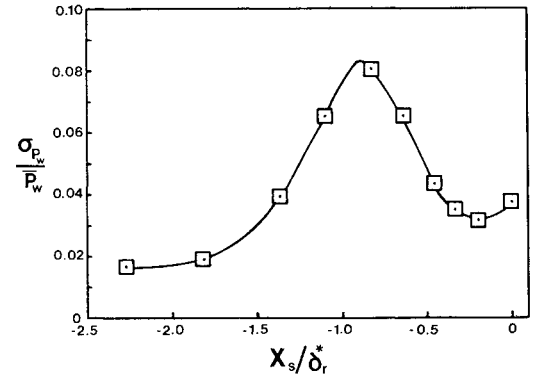

Fig. 8b Rms pressure distribution for 12 deg compression corner.

maxima is caused by unsteadiness§ in the shock-wave structure and can also be observed in the time traces of the pressure fluctuations, which exhibit intermittent behavior with the signal fluctuating between pressure levels upstream and downstream of the shock.

Examination of the time traces in the present interaction revealed no intermittent behavior and the probability density function was found to be Gaussian throughout the entire region surveyed, with a skewness of 0 ± 0.04 and kurtosis of 3.05 ± 0.07 (cf., ideal values of 0.0 and 3.0, respectively, for a Gaussian process).

This tends to suggest that the present interaction does not exhibit any unsteadiness. However, as the shock has bifurcated with a consequent spreading out of the pressure jumps across the shock, unsteadiness of the wave system may not reveal itself in a pressure peak or in an intermittent pressure signal. In fact, the cross-correlation results to be discussed suggest some degree of unsteadiness in the wave system.

It appears that the present three-dimensional interaction is fairly diffused. Note, however, that this interaction can be considered to be fairly "weak." With stronger three-dimensional interactions, i.e., larger fin angles, we may observe intermittent behavior in the pressure signals similar to that observed in the two-dimensional compression ramp studies.

Broadband Space Correlations

The broadband space correlations $R(\xi_1, \xi_2, 0)$ for the three positions where the plug was yawed are shown in Fig. 9. Although data at only three transducer separations ξ were taken, the results are sufficiently "well behaved" to allow smooth curves to be drawn through the data points [the curves are assumed to go through $R(0,0,0) = 1$]. From these curves, contour plots of $R(\xi_1, \xi_2, 0)$ can be constructed as shown in Fig. 10.

The shape of the contour plot at $X_s = -23.8\delta_r^*$ (Fig. 10a) compares favorably to that obtained by Bull[22] and by Speaker and Ailman,[15] with the transverse scale larger than the longitudinal, i.e., elliptical contours. The space correlations give an indication of the spatial scales of the pressure producing structures. The development of these structures through the interaction can be followed by observing the contours at $X_s = -8.5\delta_r^*$ and $X_s = 10.5\delta_r^*$. The structures appear to be swept in the spanwise direction and at $X_s = 10.5\delta_r^*$ the elliptical contours are aligned with the major axis at approximately 35 deg. This coincides with the surface isobar pattern, as shown in Fig. 11; the position where the yaw measurements were taken have also been indicated.

Broadband Space-Time Correlation

The broadband convection velocity of the pressure signatures U_c is usually taken to be that of a frame of reference in which the rate of decay of the space-time correlation $R(\xi_1, \xi_2, \tau)$ is least (see, for example, Willmarth and Wooldridge[23] or Wills[24]). In two-dimensional flows, the convection velocity is a function of the spacing of the transducers, the frequency range measured, and the angle $\beta = \tan^{-1}\xi_2/\xi_1$, which is the angle of the flow relative to the survey direction. The deduced convection velocity increases to an asymptotic value as the transducer spacing increases. Measurements in lower-frequency bands also give higher values of convection velocity than measurements in higher-frequency bands. The effect of β is to give a larger value of convection velocity, since two transducers will register a pressure signal in the time interval $t \cos\beta$, where t is the time taken to move the distance ξ when the transducers are aligned with the flow. The measured convection velocity U_m will then be given approximately by $U_c/\cos\beta$, where U_c is the actual convection velocity, i.e., in the flow direction. This is only a rough first-order approximation, since U_m is also a function of the transducer separation and the shape of the structures.

In three-dimensional flows, the problem of defining a flow direction occurs, since the flow above any point on the wall is

§Unsteadiness refers to comparatively low-frequency oscillation of the shock structure.

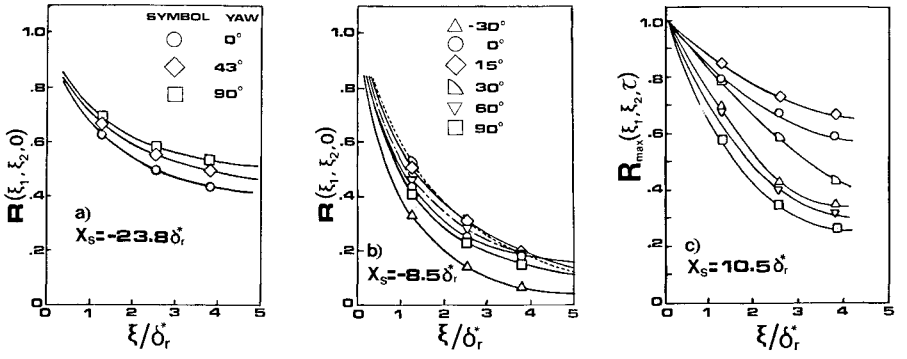

Fig. 9 Space correlation distributions at the yaw measurement locations.

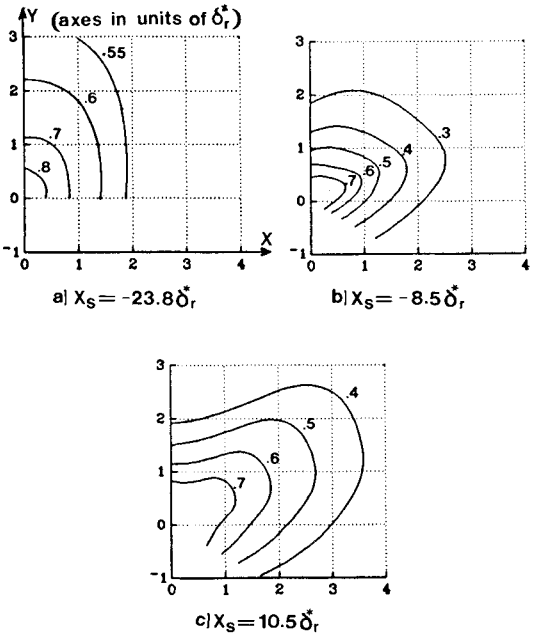

Fig. 10 Approximate contour plots of equal space correlation coefficients for the yaw measurement locations.

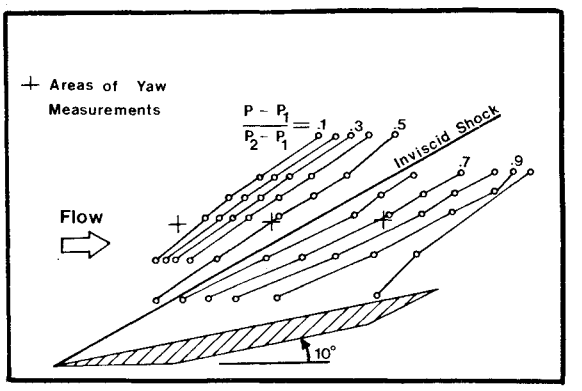

Fig. 11 Surface isobar pattern (from Ref. 5).

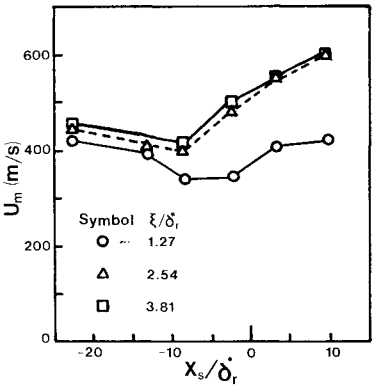

Fig. 12 Broadband convection velocities along $Y = 95.3$ mm.

yawed through a range of angles.¶ For example, the flow at $X_s = 10.5\delta_r^*$ is yawed from 10 deg at the freestream value to 55 deg at the wall. Figure 12, which shows the convection velocity for different transducer spacings along the longitudinal survey line, demonstrate this effect clearly. In an adverse pressure gradient, the convection velocity would be expected to decrease. The convection velocity distribution at the smallest transducer spacing appears to do this, but the distributions for the larger transducer spacings increase to values greater than U_e. The different trend at larger transducer spacings is due to the fact that data obtained at larger spacings would be weighted toward the larger structures, which decay more slowly and have higher convection velocities. The measurements are therefore more sensitive to β in that a given change in β would cause a larger change in U_m.

Figure 13 shows the peak values of the cross-correlations $R_{max}(\xi_1, \xi_2, \tau)$ for the three positions where yaw measurements were taken. Contour plots of R_{max}, which give an indication of the decay rates of the structures, can be constructed as shown in Fig. 14. Note that the decay rate of R_{max} increases as one moves downstream, with the decay rate at $X_s = 8.5\delta_r^*$ being greater than that at $X_s = 10.5\delta_r^*$. An "average" flow direction, or more precisely, that of the pressure producing structures, can then be defined as the direction of minimum decay of R_{max}. This direction is found to be approximately 20 deg for the results at $X_s = -8.5$ and $10.5\delta_r^*$.

An unexpected feature was observed in the cross-correlation curves at the higher yaw angles. Figure 15 shows $R(\xi_1, \xi_2, \tau)$ as a function of τ for the $X_s = 10.5\delta_r^*$ yaw survey position. As can be seen, the peak in cross correlation occurs at negative τ for the two larger transducer spacings. This suggests that the second, or "downstream," transducer is registering a pressure signal before the first transducer. The curves also appear to exhibit a second peak at positive τ. Although the value of R at the second peak is small, its appearance can be tracked and is consistent with what one would expect from the flow, i.e., a peak at positive τ. Extensive checks had discounted the likelihood that the curves were in error or were caused by some acoustic wave. The peak at negative τ suggests that a pressure disturbance is propagating at a negative angle (i.e., toward the fin).

¶Note that the consideration of the flow that is above the transducer is only a convenience since, aside for a thin subsonic layer, the flow is supersonic and the pressure signals therefore originate from upstream disturbances that are propagated along characteristics.

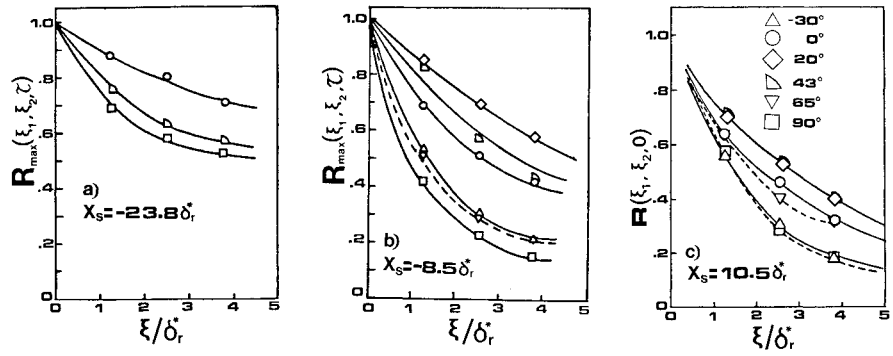

Fig. 13 Distribution of maxima in space-time correlations at the yaw measurement locations (for legend, see Fig. 9).

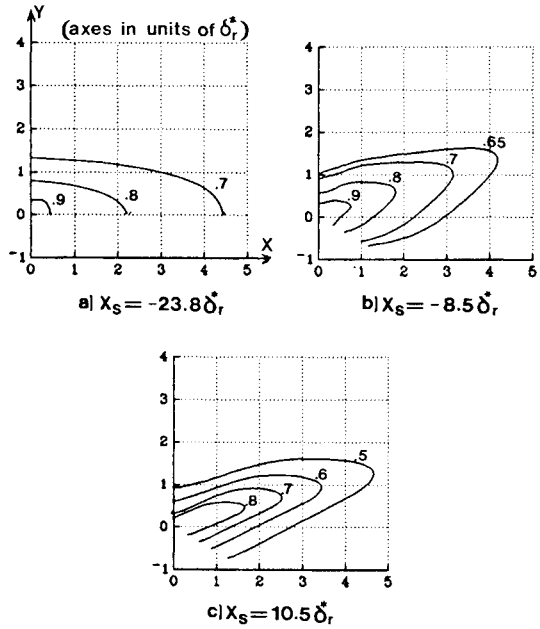

Fig. 14 Approximate contour plots of equal space-time correlation coefficient for the yaw measurement locations.

Further support for this is found in the cross-correlation curves at the yaw angle of -30 deg shown in Fig. 16. Since the mean flow varies ~ 10-55 deg, one would expect to deduce a large convection velocity U_m from the cross correlations at this yaw angle (since the transducers are aligned at a large angle to the mean flow direction). Instead, the values of U_m for the different transducer spacings range ~ 360-460 m/s, which would be the case if the transducers were registering a signal moving in the negative yaw direction.

From the yaw angle surveys of Oskam et al.,[5] the mean flow does not achieve a negative yaw angle at any stage. It is unlikely then that the peak in R at negative τ is caused by a pressure disturbance moving with the flow. The authors conjecture that this peak is caused by some fluttering motion of the shock system. From the present results, the motion appears to be approximately normal to the calculated shock angle.

The cross-correlation curves at $X_s = -8.5\delta_r^*$ also exhibit this feature, although it is not as pronounced.

Narrow Band Analysis

Figure 17 shows the narrow band convection velocities at the $X_s = -23.8\delta_r^*$ position at zero yaw angle. Also shown for comparison is the curve fitted by Bull[22] through his data. The vertical bar indicates the degree of scatter in Bull's data. Although the degree of scatter is large, it indicates the ex-

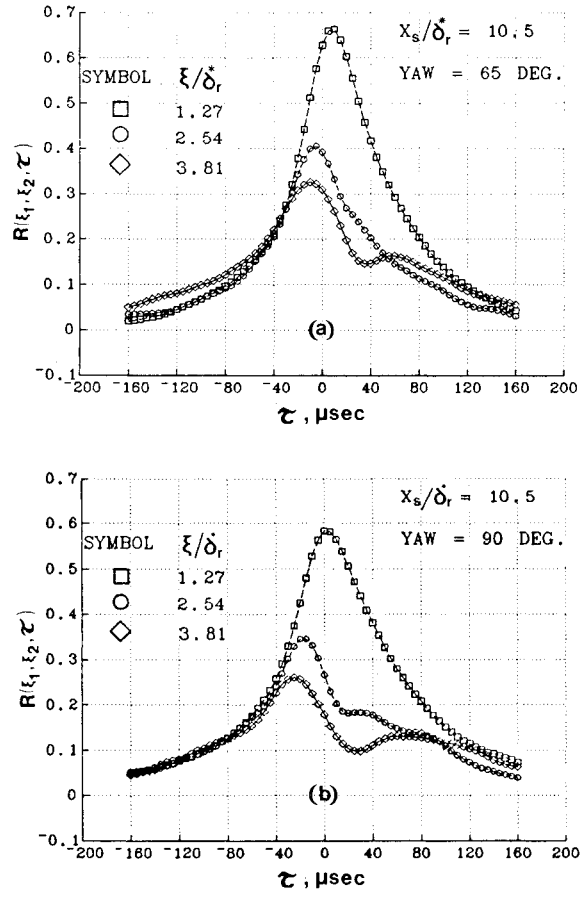

Fig. 15 Space-time correlation coefficients at $X_s = 10.5\delta_r^*$ for yaw angles of: a) 65 deg and b) 90 deg.

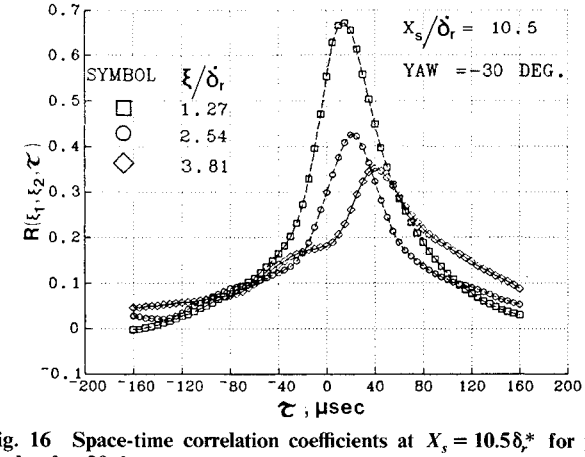

Fig. 16 Space-time correlation coefficients at $X_s = 10.5\delta_r^*$ for yaw angle of -30 deg.

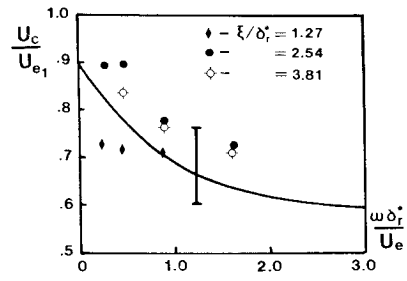

Fig. 17 Narrow-band convection velocities at $X_s = -23.8\delta_r^*$ for yaw angle of 0 deg.

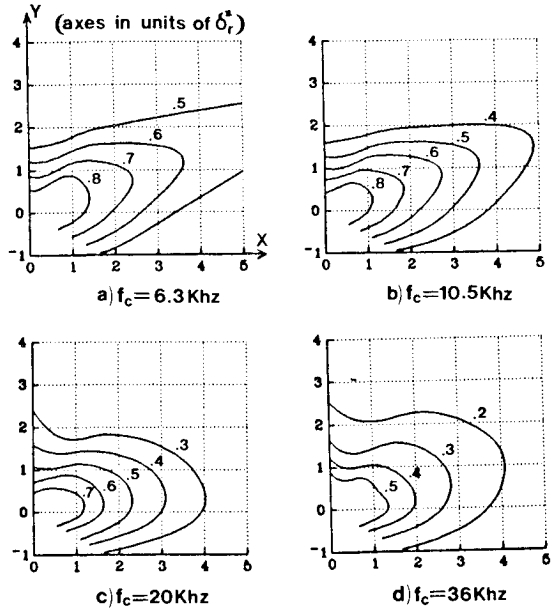

Fig. 18 Approximate contour plots of equal narrow band space-time correlation coefficient maxima at $X_s = 10.5\delta_r^*$.

pected decrease in convection velocity with increasing frequency.

Isocorrelation contours of the maxima in narrow band space-time correlations at $X_s = 10.5\delta_r^*$ are shown in Fig. 18. The contours are roughly elliptical in shape with decreasing major/minor axes ratio with increasing frequency. Note the distortion at the higher-frequency bands, which may be caused by the previously discussed unsteadiness of the shock structure. The contours at $X_s = -8.5\delta_r^*$ are similar.

Conclusion

The current experiment investigated the nature of the fluctuating wall pressures in a three-dimensional shock-wave/boundary-layer interaction. Rms pressure and space-time cross-correlation measurements were obtained in various regions of the flow and the development of these quantities was discussed.

The rms pressure distribution was found to be significantly lower than that in a two-dimensional compression corner with a shock wave of similar strength; in particular, no peak in rms pressure was found. The pressure signals also did not exhibit any intermittent behavior. This, however, does not indicate that the interaction is steady, since the shock wave bifurcates into a wave system and unsteadiness in this system would not necessarily produce a peak in the rms pressure distribution or produce intermittent pressure signals. In fact, cross-correlation analysis of the signals suggest that the wave system exhibits some degree of unsteadiness.

The development of the pressure producing structures was also revealed in contour plots of the space correlation. In the upstream incoming boundary layer, the length scale in the flow direction was smaller than that in the lateral direction; this was altered in the interaction so that the length scale in the flow direction, or more precisely, in the direction of the minimum pressure gradient, becomes larger than that in the direction normal to the flow.

Isocorrelation contours of the maxima in the space-time correlations were deduced and the contours were found to be nearly elliptical in shape with the major axis aligned approximately with the average flow direction, which was also the direction of minimum pressure gradient.

Narrow band analysis of the pressure signal was also performed. As expected, the deduced convection velocities decreased with increasing frequency bands. The isocorrelation contours of the narrow-band space-time correlations were also elliptic in shape with the major/minor axis ratio decreasing with increases in frequency.

Acknowledgments

The authors would like to acknowledge many stimulating discussions with Drs. J.-P. Dussauge and K.C. Muck and Professor A.J. Smits. This work was supported by the U.S. Air Force Office of Scientific Research under Contract F49620-81-K-0018, monitored by Dr. J.D. Wilson.

References

[1]McCabe, A., "The Three-Dimensional Interaction of a Shock Wave with a Turbulent Boundary Layer," *Aeronautical Quarterly*, Vol. 17, 1966, p. 231.

[2]Stanbrook, A., "An Experimental Study of the Glancing Interaction Between a Shock Wave and a Turbulent Boundary Layer," British Aeronautical Research Council, Rept. CP555, 1960.

[3]Kubota, H. and Stollery, J.L., "An Experimental Study of the Interaction Between a Glancing Shock Wave and a Turbulent Boundary Layer," *Journal of Fluid Mechanics*, Vol. 116, 1982, p. 431.

[4]Peake, D.J., "The Three-Dimensional Interaction of a Swept Shock Wave with a Turbulent Boundary Layer and the Effects of Air Injection on Separation," Ph.D. Thesis, Carleton University, Ottawa, Canada, March 1975.

[5]Oskam, B., Bogdonoff, S.M., and Vas, I.E., "Study of Three-Dimensional Flow Fields Generated by the Interaction of a Skewed Shock Wave with a Turbulent Boundary Layer," AFFDL-TR-75-21, 1975.

[6]Korkegi, R.H., "On the Structure of Three-Dimensional Shock-Induced Separated Flow Regions," *AIAA Journal*, Vol. 14, 1976, p. 597.

[7]Horstman, C.C., "A Computational Study of Complex Three-Dimensional Compressible Turbulent Flow Fields," AIAA Paper 84-1556, 1984.

[8]Knight, D.D., "Numerical Simulation of 3D Shock Turbulent Boundary Layer Interaction Generated by a Sharp Fin," AIAA Paper 84-1559, 1984.

[9]Stalker, R.J., "A Characteristic Approach to Swept Shock-Wave/Boundary-Layer Interactions," *AIAA Journal*, Vol. 22, 1984, p. 1626.

[10]Settles, G.S. and Teng, H.Y., "Flow Visualization of Separated 3-D Shock Wave/Turbulent Boundary Layer Interaction," AIAA Paper 82-0229, 1982.

[11]Raman, K.R., "A Study of Surface Pressure Fluctuations in Hypersonic Turbulent Boundary Layers," NASA CR-2386, 1974.

[12]Hanly, R.D., "Effects of Transducer Flushness on Fluctuating Surface Pressure Measurements," AIAA Paper 75-534, 1975.

[13]McClellan, J.H., Parks, T.W., and Rabiner, L.R., "A Computer Program for Designing Optimum FIR Linear Phase Digital Filters," *IEEE Transactions on Audio and Electroacoustics*, Vol. AU-21, No. 6, 1973.

[14]Kistler, A.L. and Chen, W.S., "The Fluctuating Pressure Field in a Supersonic Turbulent Boundary Layer," *Journal of Fluid Mechanics*, Vol. 16, 1963, p. 41.

[15]Speaker, W.V. and Ailman, C.M., "Spectra and Space-Time Correlations of the Fluctuating Pressures at a Wall Beneath a Supersonic Turbulent Boundary Layer Perturbed by Steps and Shock Waves," NASA CR-486, 1966.

[16]Chu, W.J. and Hanly, R.D., "Power and Cross Spectra and Space-Time Correlations of Surface Fluctuating Pressures at Mach Numbers between 1.6 and 2.6," AIAA Paper 68-77, 1968.

[17]Coe, C.F., "Surface Pressure Fluctuations Associated with Aerodynamic Noise," NASA SP-207, 1969, p. 409.

[18]Laganelli, A.L., Martellucci, A., and Shaw, L.L., "Wall Pressure Fluctuations in Attached Boundary-Layer Flow," *AIAA Journal*, Vol. 21, April 1983, p. 495.

[19]Schewe, G., "On the Structure and Resolution of Wall-Pressure Fluctuations Associated with Turbulent Boundary-Layer Flow," *Journal of Fluid Mechanics*, Vol. 134, 1983, p. 311.

[20]Corcos, G.M., "Resolution of Pressure in Turbulence," *Journal of the Acoustical Society of America*, Vol. 35, No. 2, 1963, p. 192.

[21]Dolling, D.S. and Or, C.T., "Unsteadiness of the Shock Wave Structure in Attached and Separated Compression Ramp Flowfields," AIAA Paper 83-1715, 1983.

[22]Bull, M.K., "Wall Pressure Fluctuations Associated with Subsonic Turbulent Boundary Layer Flow," *Journal of Fluid Mechanics*, Vol. 28, Pt. 4, 1967, p. 719.

[23]Willmarth, W.W. and Wooldridge, C.E., "Measurements of the Fluctuating Pressure at the Wall Beneath a Thick Turbulent Boundary Layer," *Journal of Fluid Mechanics*, Vol. 14, 1962, p. 187.

[24]Wills, J.A.B., "On Convection Velocities in Turbulent Shear Flows," *Journal of Fluid Mechanics*, Vol. 20, 1964, p. 417.

From the AIAA Progress in Astronautics and Aeronautics Series . . .

COMBUSTION EXPERIMENTS IN A ZERO-GRAVITY LABORATORY—v. 73

Edited by Thomas H. Cochran, NASA Lewis Research Center

Scientists throughout the world are eagerly awaiting the new opportunities for scientific research that will be available with the advent of the U.S. Space Shuttle. One of the many types of payloads envisioned for placement in earth orbit is a space laboratory which would be carried into space by the Orbiter and equipped for carrying out selected scientific experiments. Testing would be conducted by trained scientist-astronauts on board in cooperation with research scientists on the ground who would have conceived and planned the experiments. The U.S. National Aeronautics and Space Administration (NASA) plans to invite the scientific community on a broad national and international scale to participate in utilizing Spacelab for scientific research. Described in this volume are some of the basic experiments in combustion which are being considered for eventual study in Spacelab. Similar initial planning is underway under NASA sponsorship in other fields—fluid mechanics, materials science, large structures, etc. It is the intention of AIAA, in publishing this volume on combustion-in-zero-gravity, to stimulate, by illustrative example, new thought on kinds of basic experiments which might be usefully performed in the unique environment to be provided by Spacelab, i.e., long-term zero gravity, unimpeded solar radiation, ultra-high vacuum, fast pump-out rates, intense far-ultraviolet radiation, very clear optical conditions, unlimited outside dimensions, etc. It is our hope that the volume will be studied by potential investigators in many fields, not only combustion science, to see what new ideas may emerge in both fundamental and applied science, and to take advantage of the new laboratory possibilities.

Published in 1981, 280 pp., 6×9, illus., $19.50 Mem., $39.50 List

TO ORDER WRITE: Publications Order Dept., AIAA, 1633 Broadway, New York, N.Y. 10019